Targeting connexin 43 expression via scaffold mediated delivery of antisense oligodeoxynucleotide preserves neurons, enhances axonal extension, reduces astrocyte and microglial activation after spinal cord injury

Jiah Shin Chin[1,2], Ulla Milbreta[2], David L Becker[3,4] and Sing Yian Chew[2,3,5] (iD)

Abstract

Injury to the central nervous system (CNS) provokes an inflammatory reaction and secondary damage that result in further tissue damage and destruction of neurons away from the injury site. Upon injury, expression of connexin 43 (Cx43), a gap junction protein, upregulates and is responsible for the spread and amplification of cell death signals through these gap junctions. In this study, we hypothesise that the downregulation of Cx43 by scaffold-mediated controlled delivery of antisense oligodeoxynucleotide (asODN), would minimise secondary injuries and cell death, and thereby support tissue regeneration after nerve injuries. Specifically, using spinal cord injury (SCI) as a proof-of-principle, we utilised a fibre-hydrogel scaffold for sustained delivery of Cx43asODN, while providing synergistic topographical cues to guide axonal ingrowth. Correspondingly, scaffolds loaded with Cx43asODN, in the presence of NT-3, suppressed Cx43 up-regulation after complete transection SCI in rats. These scaffolds facilitated the sustained release of Cx43asODN for up to 25 days. Importantly, asODN treatment preserved neurons around the injury site, promoted axonal extension, decreased glial scarring, and reduced microglial activation after SCI. Our results suggest that implantation of such scaffold-mediated asODN delivery platform could serve as an effective alternative SCI therapeutic approach.

Keywords

Cx43, electrospinning, gap junction, nerve regeneration, neural tissue engineering

[1]Nanyang Institute of Health Technologies, Interdisciplinary Graduate School, Nanyang Technological University, Singapore
[2]School of Chemistry, Chemical Engineering and Biotechnology, Nanyang Technological University, Singapore
[3]Lee Kong Chian School of Medicine, Nanyang Technological University, Singapore
[4]Skin Research Institute Singapore, Clinical Sciences Building, Singapore
[5]School of Materials Science and Engineering, Nanyang Technological University, Singapore

Corresponding authors:
David L Becker, Lee Kong Chian School of Medicine, Nanyang Technological University, 11 Mandalay Road, 308232, Singapore
Email: david.becker@ntu.edu.sg

Sing Yian Chew, School of Chemistry, Chemical Engineering and Biotechnology, Nanyang Technological University, 62 Nanyang Drive, 639798, Singapore.
Email: sychew@ntu.edu.sg

Introduction

Gap junctions facilitate intracellular communication via the exchange of metabolites (e.g. lactate), ions (e.g. potassium ions) and secondary messengers (e.g. ATP).[1] Two opposing hemichannels in individual cells, dock to form a gap junction. Each hemichannel is made of six connexin subunits that are arranged around a central pore.[1] Connexin 43 (Cx43) belongs to the connexin family of gap-junction proteins that is encoded by 20 genes in rodents and 21 genes in humans[2] and it is the most ubiquitous. Its expression is dynamically regulated after wounding in many tissues, including cornea, skin, and nervous tissue.[3–7] Notably, expression of Cx43 can be found throughout the adult mammalian central nervous system (CNS) with predominant association in astrocytes and activated microglia.[7–11] Under normal physiological conditions, in the absence of any injury to the CNS, Cx43 is involved in homeostatic buffering, providing metabolic support for neurons, synchronising astrocyte networks, regulating vascular components, and modulating synaptic activity and plasticity.[12]

Injury to the CNS provokes an inflammatory reaction and the secondary damage can result in further tissue damage and destruction of neurons away from the injury site.[13,14] In models of neurotrauma such as traumatic brain injury (TBI) and spinal cord injury (SCI), a significant increase in Cx43 protein was observed.[15,16] Of note, the spread and amplification of cell death signals was reported to have occurred through these gap junctions.[17] Dead neurons cannot be easily replaced. Hence, neuroprotection is key to minimising damage after CNS injury. The administration of pan gap junction blockers in these models were identified to be neuroprotective and hence serve as potential therapeutics.[18] Although proven to be neuroprotective, gap junction blockers have unacceptable side-effects in the CNS as they can interfere with other important cellular processes such as synaptic transmission and calcium release.[19–21] Nucleic acid- based agents could provide greater specificity of action. However, nucleic acid delivery to the CNS remains challenging.

Antisense oligodeoxynucleotides (asODNs) allow the specific downregulation of Cx43 protein expression.[22] Cx43 specific asODN is a single stranded DNA sequence of 30 deoxynucleotides with an unmodified backbone that binds specifically to complementary sequences on an accessible region of the Cx43 mRNA – forming a DNA–RNA duplex that will be cleaved by RNase H and consequently, limiting the synthesis of Cx43.[22] Unmodified asODNs have relatively short half-life inside cells (about 30 min) and are more rapidly broken down in contact with serum[23] thereby reducing the chance of off target effects.

After an SCI injury, expression of Cx43 on astrocytes and activated microglia remain high even up to 4 weeks post-injury.[24] Cx43-immunoactivity was reported to be high in areas associated with neuronal loss while in areas where neurons were preserved, Cx43 levels remained normal.[25] We hypothesise that transient Cx43 downregulation might be insufficient to minimise the spread of cell death signals and prevent neuronal loss away from the lesion sites. Building on these well-established findings, we sought to improve the delivery of Cx43 asODNs for long-term neuroprotective purposes, using SCI as a proof-of-concept and an extended application.

Despite the success reported from various clinical trials,[26–28] the use of asODNs as therapeutics remains largely hindered by the lack of suitable delivery platforms catered to the injury environment. Nanocarriers are delivery vehicles that can protect asODNs while facilitating their cellular internalisation.[29,30] Although such vehicles have demonstrated success in liver diseases and anti-cancer treatments,[30] these nanocarrier approaches do not provide topographical guidance necessary to guide axonal outgrowth after an SCI. Hydrogels, such as F127 Pluronic gel, have also been widely adopted to deliver asODNs, in particular Cx43 asODNs.[11,31] Although cells could reside in the hydrogel matrix, distinct topographical cues to guide outgrowth of axons were absent. Moreover, F127 Pluronic gel has a short half-life and degrades within 24 h. Hence, the downregulation of Cx43 expression cannot be sustained, which is a limitation in a chronically inflamed environment such as SCI.

Here, we utilised a fibre-hydrogel scaffold that guides axonal ingrowth[32–34] to deliver Cx43 asODNs *in vivo*. Specifically, we examined the release kinetics of asODNs from this platform and assessed how such sustained asODN release can prevent loss of neurons, enhance axonal extension, modulate glial scarring, and reduce microglial activation after SCI.

Experimental section

Materials

2,2,2-trifluoroethanol (TFE), sodium hydroxide (NaOH), paraformaldehyde (PFA), sucrose, Triton X-100, concentrated hydrochloric acid, sodium carbonate, magnesium sulphate, heparin sodium salt, Limonene and acetic acid were purchased from Sigma-Aldrich. Cx43 Antisense Oligodeoxynucleotides (asODN, Sequence: GTAATTGCGGC ACGAGGAATTGTTTCTGTC) was synthesised by Sigma-Aldrich. 3 ml luer lock syringe and 21-gauge needles were purchased from Becton, Dickinson and Company (BD). Rat-tail type 1 collagen was purchased from Corning. Commercial grade 100% ethanol was purchased from Aik Moh paints and chemicals and diluted to two other concentrations – 70% and 95% with distilled water. Phosphate-buffered saline was purchased at 10x concentration from Bio Basic and diluted to 1x concentration for use in this study (PBS). Tissue-Tek OCT compound was purchased from Sakura Finetek. Haematoxylin and alcoholic eosin Y 515 were purchased

from Leica Biosystems. Fluoromount-G was purchased from Abcam. Quant-iT™ OliGreen™ ssDNA Assay Kit, Alexa Fluor 488 goat anti rabbit, Alexa Fluor 555 goat anti mouse, Alexa Fluor 555 goat anti chicken, Alexa Fluor 633 goat anti rabbit, 4′,6-diamidino-2-phenylindole (DAPI) and bovine serum albumin (BSA) were obtained from Life Technologies. Chicken anti-NF200 was purchased from Biolegend. Rabbit anti-glial fibrillary acidic protein (GFAP) was obtained from DAKO. Mouse anti-Ox42 was purchased from Bio-Rad. Neurotrophin-3 (NT-3) was obtained from PeproTech.

Fibre-hydrogel scaffold fabrication

Fibres. Poly (caprolactone-co-ethyl ethylene phosphate) (PCLEEP) copolymer (Mw = 59,102, Mn 25,542) was a gift from Dr. Yucai Wang's lab. It was synthesised as reported previously.[35] PCLEEP was dissolved in TFE at 33% (wt./wt.) and settled overnight before use to ensure homogeneity. A two-pole air gap electrospinning technique was adopted to fabricate aligned PCLEEP fibres (Figure 1(a)). Briefly, the electrospinning solution was first loaded into a 3 ml syringe and then capped with a 21-gauge blunt-tipped needle. This electrospinning solution was subsequently extruded at a constant flow rate of 1.5 ml/h by a syringe pump. A positive charge (+8 kV) was applied to the blunt-tip needle while a negative charge (−4 kV) was applied to the two-pole air-gap collector. PCLEEP fibres were deposited within a 5.0 cm air gap area that was between the stationary poles. Each layer of fibres was obtained after 6 min and 30 s of spinning before combining into a stack that contained seven sets (Figure 1(b)). All fibre layers were UV sterilised for 30 min prior to stacking and rolling these layers into a bundle of fibres. A sterilised cylindrical mould (8.0 mm in length and 3.5 mm in inner diameter) was used to set the fibre bundle in the core region before adding the collagen matrix – fibre bundle was embedded within the collagen matrix.

Collagen matrix. Rat-tail type 1 collagen matrix was used to fabricate the hydrogel matrix. All procedures were conducted in accordance with the manufacturer's protocol. Briefly, 10x PBS, 1.0 N NaOH, de-ionised (DI) water and type 1 collagen stock solution were added into a sterile 600 μl micro-tube in the listed order and mixed gently to get a final collagen concentration of 3.0 mg/ml. Collagen matrix was incorporated either with growth factors only or a combination of growth factors with Cx43 asODN. Growth factors were incorporated into this matrix to promote infiltration of neurofilaments. NT-3 was reconstituted in 0.1% BSA and 400 μg/μl heparin at 1:1 (v/v) to arrive at a stock concentration of 2 μg/μl. 4 μl of NT-3 stock solution was used to substitute 4 μl of DI water in the 250 μl collagen mixture per 8 mm mould. Hence, a total of 8 μg of NT-3 was loaded into

this mixture. Cx43 asODN was reconstituted in nuclease-free water to achieve 6 mM stock concentration. Then, 18 μl of Cx43 asODN stock solution was used to further substitute 18 μl of DI water in the 250 μl collagen mixture per 8 mm mould. Thus, 1 mg of Cx43 asODN was loaded into this mixture for the matrix containing both growth factors and Cx43 asODN. This was the maximum possible mass of asODN that can be added into the collagen matrix without affecting stability of the structure. The theoretical loading of both NT-3 and Cx43 asODN, per animal, were based of our previous work.[11,34] Table 1 depicts the mass of growth factors and Cx43 asODN used per animal. All collagen mixtures were kept on ice until dispensed into the moulds that contained the electrospun fibre bundle in the core region. Hydrogel formation occurred at room temperature for 30 min before freezing the scaffolds at −20°C for 4 h prior to overnight lyophilisation. Subsequently, scaffolds were cut into 2 mm long lengths under sterilised conditions before implantation into each animal.

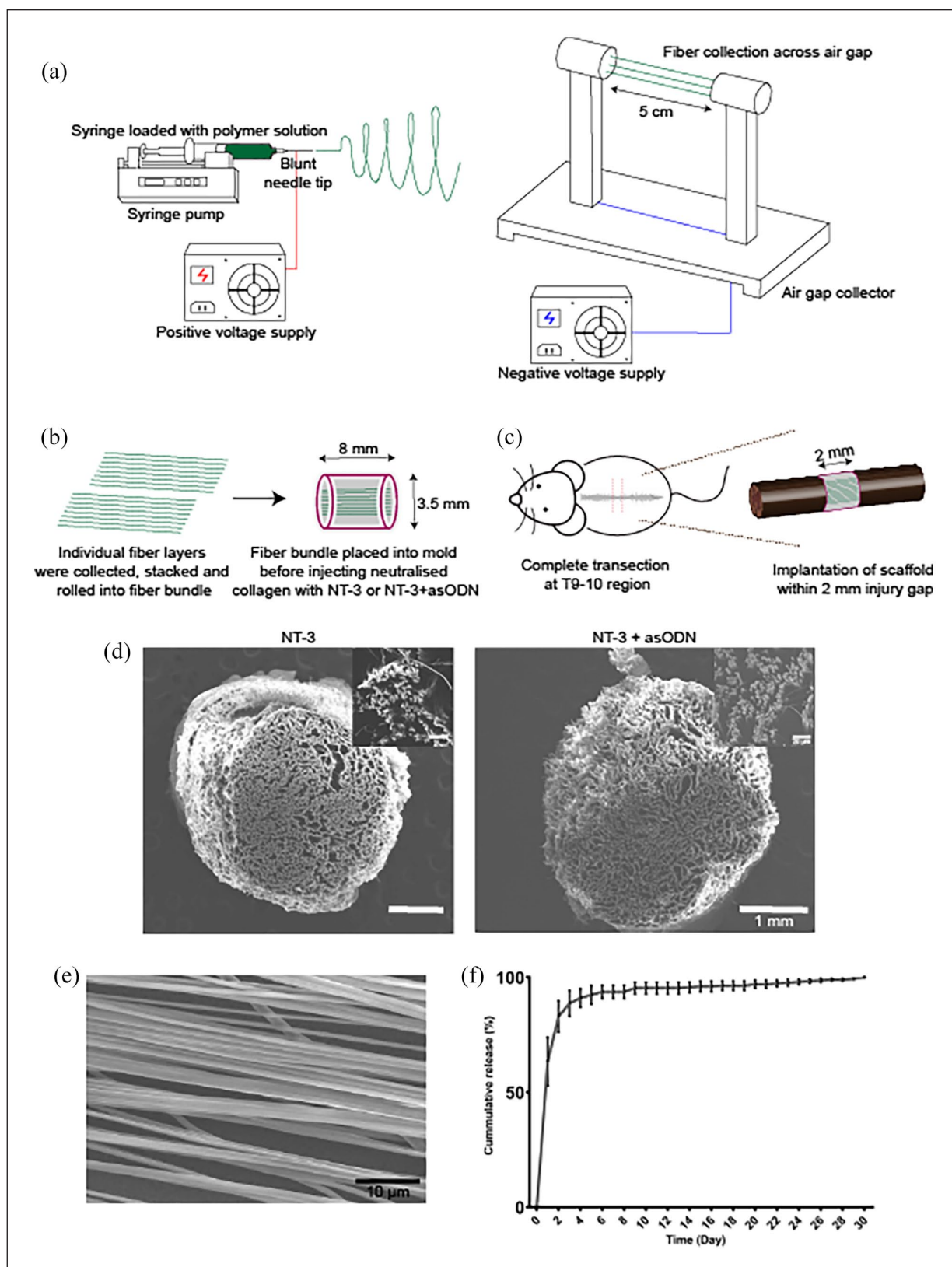## Physical characterisation of fibre-hydrogel scaffolds

The morphology of the aligned PCLEEP fibre layers and fibre-hydrogel scaffolds were evaluated by scanning electron microscopy (SEM) (JOEL, JSM-6390LA, Japan) under an accelerating voltage of 10 kV after sputter-coating with platinum at 10 mA for 100 and 120 s, respectively. The diameter of PCLEEP fibres were quantified by measuring at least 100 fibres per layer. Three fibre layers were quantified to arrive at an average fibre diameter value. All measurements were performed with ImageJ software (NIH, USA).

Quantification of asODN loading and release

Each NT-3 + asODN loaded scaffold (2.01 ± 0.09 mg) was incubated in 1 ml of 1X PBS at 37°C. At each time point, 500 μl of supernatant was collected and replaced by an equal volume of fresh 1X PBS. The amount of asODN release was measured using the Quant-iT™ OliGreen™ ssDNA Assay Kit, following manufacturer's protocol. The percentage of cumulative release of asODN was finally presented as mean ± standard deviation (S.D.)

To evaluate the experimental loading efficiency of asODN, NT-3 + asODN scaffolds (*n* = 3) were dissolved in 1 ml of TFE. Thereafter, 200 μl of 1X PBS was added. After shaking for 30 min, the aqueous phase was collected, and this process was repeated three times. The amount of asODN within the extracted aqueous solution was then determined using the OliGreen assay. Subsequently, the experimental loading efficiencies were computed using the following equation:

$$Loading\ efficiency = \frac{Total\ asODN\ released + Total\ asODN\ extracted}{Total\ theorectical\ asODN\ loading} \times 100\%$$

Figure 1. Schematic of (a) air-gap electrospinning setup, (b) fibre-hydrogel scaffold fabrication and (c) implantation of scaffold into 2 mm spinal cord injury gap. Physical characterisation of fibre-hydrogel scaffolds. (d) SEM images of cross-section of fibre-hydrogel scaffolds showing that aligned fibres were well orientated and uniformly distributed in the collagen matrix. (e) SEM image of aligned electrospun PCLEEP fibres. (f) Cumulative release profile of asODN from fibre-hydrogel scaffolds over 30 days.

Table 1. Mass of growth factors and Cx43 asODN used per animal.

Collagen matrix	Mass of NT-3 (µg)	Mass of Cx43 asODN (µg)
Growth factors only (NT-3)	2	0
Combination of growth factors with Cx43 asODN (NT-3 + asODN)	2	250

Spinal cord complete transection and scaffold implantation

All animal procedures were approved and performed in accordance with the Institutional Animal Care and Use Committee (IACUC) in Nanyang Technological University (IACUC Project Number A19005). Female Sprague Dawley rats were obtained from InVivos Pte. Ltd. (Singapore) and used in experiments at 7–9 weeks old (200–250 g). Animals were randomly divided into two groups to receive scaffolds loaded with NT-3 or NT-3 + asODN.

Anaesthesia was induced using intraperitoneal injection of ketamine (73 mg/kg) and xylazine (7.3 mg/kg). Animals were injected subcutaneously with 0.05 mg/ml buprenorphine as analgesia before the surgery. Before incision, the surgical field was shaved, cleaned with 70% ethanol and further disinfected with betadine. An incision on the skin was made above the thoracic level to expose the vertebra at the T8-T11 level. Subsequently, the T9 vertebra was located and a dorsal laminectomy was performed at the T9-T10 level. The dura was then opened before performing a 2 mm complete transection on the spinal cord with a pair of fine micro scissors. Thereafter, the respective scaffolds were implanted into the incision site – reconnecting the rostral and caudal parts of the resected spinal cord (Figure 1(c)). Of note, all scaffolds were randomised with allocation concealment and the sole investigator who conducted the surgery was blinded to the contents of the scaffolds. To close the incision, the dura was first sutured before covering the injury area with a 50 µm thick PCL film. Afterwards, the surrounding muscle was sutured, and the skin was closed with wound clips. Bladders were manually expressed at least twice daily until bladder function recovered.

Tissue harvesting and processing

At 4 weeks post-injury, all animals were perfused with 0.9% saline followed by ice cold 4.0% PFA. After perfusion, 1.5 cm of spinal cords (inclusive of the injury site) were dissected and further post-fixed for 2 h with 4.0% PFA at 4°C. Tissues were cryoprotected by transferring fixed tissues into 15% sucrose for 24 h followed by 30% sucrose at 4°C until cryosectioned. Spinal cord samples were sectioned in the coronal plane into 20 µm thick sections before directly mounting the sections onto poly-lysine coated glass slides.

Quantification of neurons from Haematoxylin and eosin-stained spinal cord sections

Haematoxylin and eosin (H&E) staining. All staining was performed with an autostainer (Leica Biosystems, ST5010 Autostainer XL, Germany). Frozen spinal cord sections were gently rinsed with 1x PBS to remove residual OCT compounds. Sections were then immersed in 100% ethanol for 2 min, a second container of 100% ethanol for 2 min, 95% ethanol for 2 min, a second container of 95% ethanol for 2 min, 70% ethanol for 2 min and rinsed in a container of running tap water for 2 min to rehydrate the tissues. Thereafter, sections were submerged in haematoxylin for 1 min and rinsed in a container of running tap water for 3 s to remove excess dye. Sections were then immersed in 0.3% acid alcohol (0.3% (v/v) concentrated hydrochloric acid, 70% (v/v) ethanol and 29.97% (v/v) distilled water) and further rinsed in running tap water for 2 min to remove any background staining. To enhance the contrast of the haematoxylin stain, sections were dipped into Scott's tap water (0.5% (w/v) sodium bicarbonate and 5% (w/v) magnesium sulphate dissolved in distilled water) for 5 s before rinsing the sections again with running tap water for 2 min. Haematoxylin-stained sections were then immersed into alcoholic eosin Y 515 for 2 min. Subsequently, sections were submerged in 70% ethanol for 2 min, 95% ethanol for 2 min, a second container of 95% ethanol for 2 min, 100% ethanol for 2 min, a second container of 100% ethanol for another 2 min and Clearene for 2 min to dehydrate the sections. Slides with stained sections were then individually removed, covered with one drop of Limonene and then sealed using a coverslip.

Quantification of neurons. Images of H&E-stained sections were obtained using a brightfield microscope (Leica, DMi8, Germany) at 20x magnification and automatically stitched using Leica LAS X software to obtain tilescan images of these tissue sections. Whole tissue sections were analysed in a blinded fashion using Zeiss Zen Black software (Carl Zeiss, Germany) where regions of interest (1500 µm by 1500 µm) were exported for further quantification of neurons per field of view in Image J. One tissue slice per animal, at the middle of the spinal cord, was chosen for analysis to capture the maximum width of the implanted scaffold. Four regions of interests were exported: 1 mm away from scaffold boundary at both rostral and caudal ends as well as 200 µm away from scaffold boundary at both rostral and caudal ends. Neurons were identified based on their size and location within the grey matter.[36] Notably, damaged neurons were not included in quantification. Healthy and damaged neurons were identified based on their sizes and appearance of nuclei[38].

Immunohistochemistry

Immunohistochemistry was performed to evaluate axonal ingrowth, cyst formation, glial scarring, Cx43 protein

Table 2. Details of primary and secondary antibodies.

Antibody		Dilution	Catalogue number
Primary	NF-200 (Chicken)	1:1000	Biolegend (822601)
	GFAP (Rabbit)	1:1000	DAKO (Z0334)
	Cx43 (Rabbit)	1:1000	Sigma (C6219)
	Ox42 (Mouse)	1:100	Bio-Rad (MCA275G)
Secondary	Goat anti-Chicken, Alexa Fluor 555	1:1000	Life Technologies (A-21437)
	Goat anti-Rabbit, Alexa Fluor 488	1:1000	Life Technologies (A-11034)
	Goat anti-Rabbit, Alexa Fluor 633	1:1000	Life Technologies (A-21070)
	Goat anti-Mouse, Alexa Fluor 555	1:1000	Life Technologies (A32727)

expression and the presence of microglia. All steps were performed at room temperature unless otherwise mentioned. The frozen spinal cord sections were first gently rinsed with 1X PBS to remove residual OCT compound. Enzymatic antigen retrieval was conducted on sections that were stained for Cx43 protein expression and microglial activity to enhance the staining and reduce background signals. Two drops of Histo/Zyme were added to each of these sections and incubated for 5 min. Histo/Zyme was rinsed with 1X PBS to remove all residues. All sections (treated with or without antigen retrieval) underwent the subsequent steps. Sections were permeabilised by treating with 0.3% Triton X-100 for 5 min and then incubated in 10% goat serum for 1 h to reduce non-specific antibody binding. Thereafter, the sections were incubated overnight with primary antibodies diluted in 5.0% goat serum at 4°C. These sections were subsequently washed 3 times with 1X PBS and incubated with the respective secondary antibodies for 1.5 h. Similarly, secondary antibodies were diluted in 5.0% goat serum. Nuclear counterstaining was performed by incubating these sections with DAPI (1:1000) for 15 min after the secondary antibodies. Details of primary and secondary antibodies used along with their dilutions are listed in Table 2. All stained slides were mounted with Fluoromount-G and sealed with coverslips.

Fluorescent microscopy

Images of DAPI, NF-200 and GFAP stained spinal cord sections were captured at a 10x magnification using a fluorescent microscope (Leica, DMi8, Germany) and automatically stitched using LAS X software (Leica, Germany) to obtain tilescan images of these tissue sections. Polarised light images were taken concurrently to capture the scaffold implanted at the injury site in these sections. For each animal, at least three sections were imaged (one section at the maximum width of the implanted scaffold, another section 40 μm before the maximum width of the implanted scaffold and the last section 40 μm after the maximum width of the implanted scaffold). The sections were chosen with respect to the maximum width of the implanted scaffold to evaluate the response of the injury to the scaffold.

Quantification of axonal ingrowth. The scaffold area was identified and traced from these polarised light images before quantifying the pixel area of NF-200 within this scaffold area using Image J (NIH, USA). The percentage of scaffold stained with NF-200 was calculated based on the following equation:

$$Percentage\ of\ scaffold\ stained\ with\ NF-200$$
$$= \frac{Total\ NF-200\ positive\ pixel\ area}{Scaffold\ area} \times 100$$

Size measurement of cystic cavity. Cell-free areas in the lesion sites rostral and caudal to the scaffold were identified as cystic cavities. Images of GFAP-stained sections were cross-referenced with DAPI images of the respective spinal cord section and thresholded to reveal these cell-free areas. Subsequently, the size of these cavities was highlighted and measured using Image J. The sum of these cavity areas was tabulated for each tissue section. At least three sections were quantified and averaged.

Extent of glial scarring. GFAP-positive area in the scar areas rostral and caudal to the scaffold was measured. The dense lining of GFAP-positive astrocytes in the lesion sites rostral and caudal to the scaffold was identified as the glial scar border. Subsequently, based on an established protocol, a region of interest within 500 μm from the glial scar border was demarcated.[37] Using ImageJ, a freehand line was drawn along the glial scar border and this line was then translated 500 μm away from the scaffold. The region flanked within these two lines was defined as the region of interest where the following equation was applied:

$$Percentage\ of\ GFAP + area\ within\ 500\ \mu m\ of\ scaffold\ interface = \frac{Total\ GFAP\ positive\ pixel\ area}{Area\ of\ region\ of\ interest} \times 100\%$$

Cystic cavities were excluded from this analysis. Both rostral and caudal glial scars were quantified. At least three sections were quantified and averaged.

Confocal microscopy

Single optical section images of DAPI, Cx43 and Ox42 stained spinal cord sections were acquired using a confocal microscope (Leica, SP8, Germany) with a 40x oil objective. This optical section was chosen based on the z slice with maximum Cx43 signal with the primary objective of evaluating changes to Cx43 expression with asODNs treatment and consequently, the activation state of microglial. Fluorophores were excited sequentially (DAPI using 405 nm wavelength laser, Alexa 488 using a 488 nm wavelength laser and Alexa 555 using a 555 nm wavelength laser). 8-bit images were acquired using a frame average of 5 at a resolution of 1024 by 1024 pixels. Image acquisition settings were adjusted with reference to NT-3 treated spinal cord sections to prevent oversaturation and these settings remained identical between the treatments and across all sections to allow comparison to be made during image analysis. Imaging was performed at three regions: scaffold boundary at the rostral end, within the centre of the scaffold and scaffold boundary at the caudal end. At least three sections per animal were imaged at these regions.

Quantification of Cx43 protein expression. Cx43 protein expression was quantified by counting positive pixel area from images of Cx43 stained spinal cord sections using Image J using the method outlined by a previous study.[4] All images were identically thresholded prior to analysis. The total number of cells per field of view was counted from the corresponding DAPI images. Cx43 protein levels were expressed and calculated with the following equation:

$$Cx43\,area\,per\,nuclei$$
$$=\frac{Total\,Cx43\,positive\,pixel\,area}{Total\,cell\,count\,per\,field\,of\,view}\times100\%$$

Quantification of Ox42 positive cells. Ox42 stains integrin alpha M which is involved in interactions with macrophages and is used here to recognise microglia[41]. Images of Ox42 stained spinal cord sections were overlapped with the corresponding DAPI images and cells with defined Ox42 cytoplasmic expression were identified as Ox42 positive cells. The total number of cells per field of view was counted from the corresponding DAPI images. The percentage of Ox42 positive cells per field of view were quantified with this equation:

$$Percentage\,of\,Ox42\,positive\,cells$$
$$=\frac{Number\,of\,Ox42\,positive\,cells}{Total\,cell\,count\,per\,field\,of\,view}\times100\%$$

Statistical analysis

Statistical analysis was carried out using GraphPad Prism software. All results were presented as mean ± standard deviation. The Brown-Forsythe test was used to test for equal variances while the Shapiro–Wilk test was used to test for normality. If the variances of the groups were equal and normally distributed, One-way ANOVA and Tukey's Post-hoc tests were used to compare the means of more than two samples. Where variances were not equal, the non-parametric tests, Kruskal Wallis and Mann-Whitney tests, were used.

Results

Sustained release of Cx43sODNs from fibre-hydrogel scaffolds

Topographical cues were provided to neurons to guide axonal outgrowth. This was achieved through aligned fibres that were supported by the collagen hydrogel, formulating a 3D implantable structure at the SCI injury site. Figure 1(d) shows the cross-sectional view of fibre-hydrogel scaffolds that were loaded with NT-3 only or with both NT-3 and Cx43asODN. The presence of the collagen hydrogel did not compress the fibres or induce fibre fusion. Instead, the fibre orientation and alignment were preserved. This observation is consistent even in the presence of Cx43asODN. The average diameter of these aligned fibres was $1.17 \pm 0.23\,\mu m$ (Figure 1(e)). Besides topographical cues, the fibre-hydrogel scaffolds also delivered biochemical signals. Specifically, Cx43sODN was delivered alongside with NT-3 as previous SCI studies have suggested that the presence of NT-3 is crucial to promote neuronal survival, axonal sprouting, and regeneration.[33,40–43] Through our release kinetics study, we observed that these NT-3 + Cx43sODN loaded scaffolds (Cx43sODN loading efficient of $2.56 \pm 0.61\%$) displayed burst release profiles within the first 3 days where ~80% of the loaded Cx43sODN was released (Figure 1(f)). Thereafter, ~15% of these loaded Cx43sODN was released over the next 20 days before its release started to plateau at Day 25 (Figure 1(f)).

Scaffold-mediated delivery of Cx43sODNs preserved neurons around injury site after SCI

To evaluate the efficacy of delivering Cx43asODNs via scaffolds, histological examination was conducted on the excised spinal cord tissues with scaffolds implanted at the SCI injury site. In particular, the number of neurons near and far away from the injury border was examined (Figure 2(a)). We observed distinct neurons in the NT-3 + Cx43asODN treated group at regions both near and far away from the injury border (Figure 2(b)). This is unlike
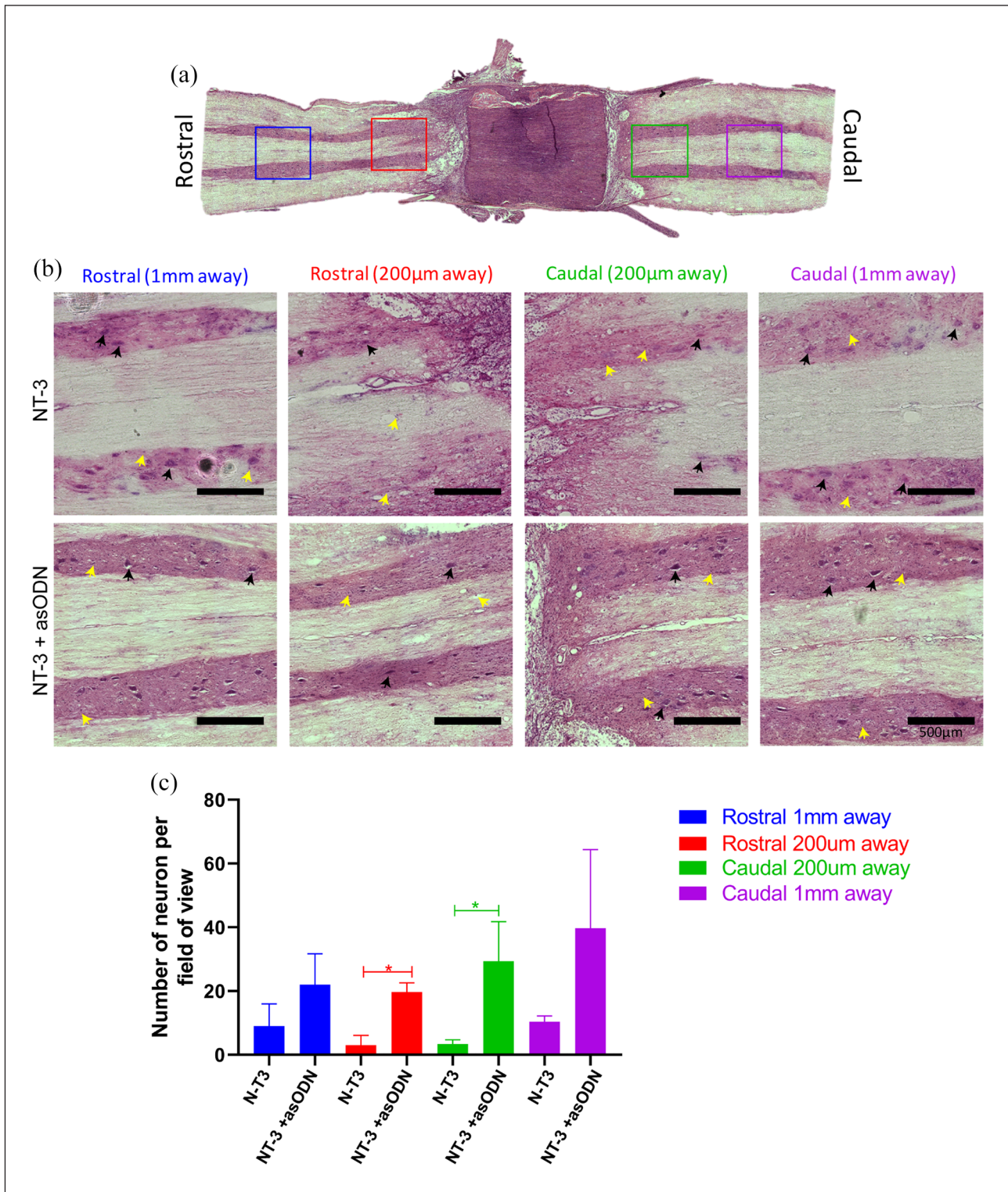
Figure 2. ASODN treatment preserved neurons after SCI. (a) H&E image of a spinal cord section, with scaffold implanted at injury site, as a representative image to show cropped regions for quantification. Blue box: Rostral, 1 mm away from scaffold interface. Red box: Rostral, 200 μm away from scaffold interface. Green box: Caudal, 200 μm away from scaffold interface. Magenta box: Caudal, 1 mm away from scaffold interface. (b) Representative H&E images of the cropped regions. Black arrows point to examples of cell that are considered as neurons. Yellow arrows point to other cell types which are significantly smaller than the identified neurons. (c) Quantification of number of neurons per field of view. More neurons were observed with asODN treatment especially at the regions near to the injury site (i.e. 200 μm away from scaffold interface). Data suggested that asODN treatment plays a role in neuron preservation after SCI. Mann Whitney test ($n = 3$, where n represents 1 biological repeat). *: $p < 0.05$.

the NT-3 treated group where neurons appeared to be undergoing cell death especially at regions near the injury border (Figure 2(b)). Furthermore, we found significantly more neurons at the regions near the injury border in NT-3 + Cx43asODN treated group ($p < 0.05$, Figure 2(c)).

Scaffold-mediated delivery of Cx43asODNs promoted axonal extension after SCI

Axonal extension from injury borders were examined with axonal marker NF-200 (Figure 3(a)). We found that NT-3 alone was insufficient to stimulate robust axonal ingrowth into the scaffold after complete spinal cord transection (Figure 3(b)). In contrast when NT-3 was coupled with Cx43asODN, extensive axonal ingrowth into the scaffolds was observed ($p < 0.01$, Figure 3(b) and (c)). Notably, these axonal extensions were well distributed within the scaffolds. In addition, we observed that these axons regenerated along the aligned fibres and were parallel to the spinal cord (Figure 3(b)).

Scaffold-mediated delivery of Cx43asODNs modulated glial scar formation but did not significantly reduce cystic cavity formation after SCI

Cystic cavity formation and glial scarring were analysed to understand the effect of Cx43asODN on host-implant integration. We first measured the size of the cystic cavities at the injury border to examine the extent of cavity formation around the scaffolds (Figure 4(a) and (b)). No significant difference was observed in the size of cavity formation between both treatment groups ($p = 0.8701$, Figure 4(b) and (c)). Subsequently, we went on to evaluate the extent of glial scarring around the scaffolds based on the expression of the reactive astrocyte marker, GFAP. A clear GFAP-positive glial scar was observed at the injury sites for both treatment groups 4 weeks after scaffold implantation (Figure 4(d)). A region of interest (ROI) was defined within 500 μm from the glial scar border and the GFAP-positive area proportional to this ROI was measured. We observed significantly reduced glial scarring at the injury borders with Cx43asODN treatment after SCI ($p < 0.01$, Figure 4(d) and (e)).

Scaffold-mediated delivery of Cx43asODNs reduced Cx43 expression and decreased microglia activation after SCI

To confirm the efficacy of delivering asODNs via our scaffolds, we exam suggested that the presence of NT ined the Cx43 protein expression at the injury borders and within the scaffold. Generally, we observed lower Cx43 protein expression at all regions for Cx43asODN treated group ($p = 0.0831$ for the injury border at rostral end and $p = 0.0573$ within the scaffold, Figure 5(b) and (c)). Downregulation of Cx43 was significantly enhanced at the injury border at the caudal end ($p < 0.05$, Figure 5(b) and (c)).

Connexin expression in microglia depends heavily on their state of activation. In their resting state, Cx43 protein expression is rarely detected.[11] Upon CNS injury, microglia shift from resting to an activated state causing Cx43 expression to increase.[11] During chronic CNS damage, activated microglia behave as uncontrolled sources of inflammatory mediators that cause neuronal damage.[43,44] Hence, regulating microglial activation could dampen secondary damage to the injured CNS. We studied the activation of microglia after SCI in the presence of Cx43asODN treatment. Reduced expression of Cx43 protein with Cx43asODN treatment was observed to be correlated to the reduction in microglial activation ($p < 0.05$ for the injury border at rostral end, $p < 0.0001$ within the scaffold and $p < 0.01$ for the injury border at the caudal end, Figure 5(c) and (d)).

Discussion

Neuroprotection is key to minimising secondary damage after spinal cord injury so as to prevent further destruction of neurons away from the local injury site.[45,46] Although there were several attempts to minimise the secondary damage after SCI, the clinical efficacy of these neuroprotective treatments when tested on humans remains controversial.[47,48] Gap junction communication has been associated with the spread of inflammatory mediators and cell death signals.[17] To suppress the spread of damage to intact tissues, from the injury sites, nucleic acids that target the expression of these gap junctions have been used. Unlike the most commonly used pharmacological gap-junction blockers,[19–21] these nucleic acids have greater specificity and minimal side effects in the CNS. However, delivery of these nucleic acids to the CNS remains challenging. Furthermore, to the best of our knowledge, there is a lack of research on scaffold-mediated nucleic acid delivery approaches that also provide topographical cues to support axonal outgrowth while offering neuroprotection. Correspondingly, this study highlights the use of scaffolds to deliver antisense oligodeoxynucleotides, targeting Cx43 protein expression, that modulates secondary neuronal damage while promoting and guiding axonal outgrowth from the injury border.

Current asODN delivery strategies have largely been confined to the use of nanocarriers.[26–30] Although some of these nanocarriers have achieved success in clinical settings, such nanocarrier approaches are unable to satisfy the unique requirements of the harsh SCI environment. Specifically, asODNs targeted at improving the SCI condition have to survive the chronically inflamed environment post SCI.
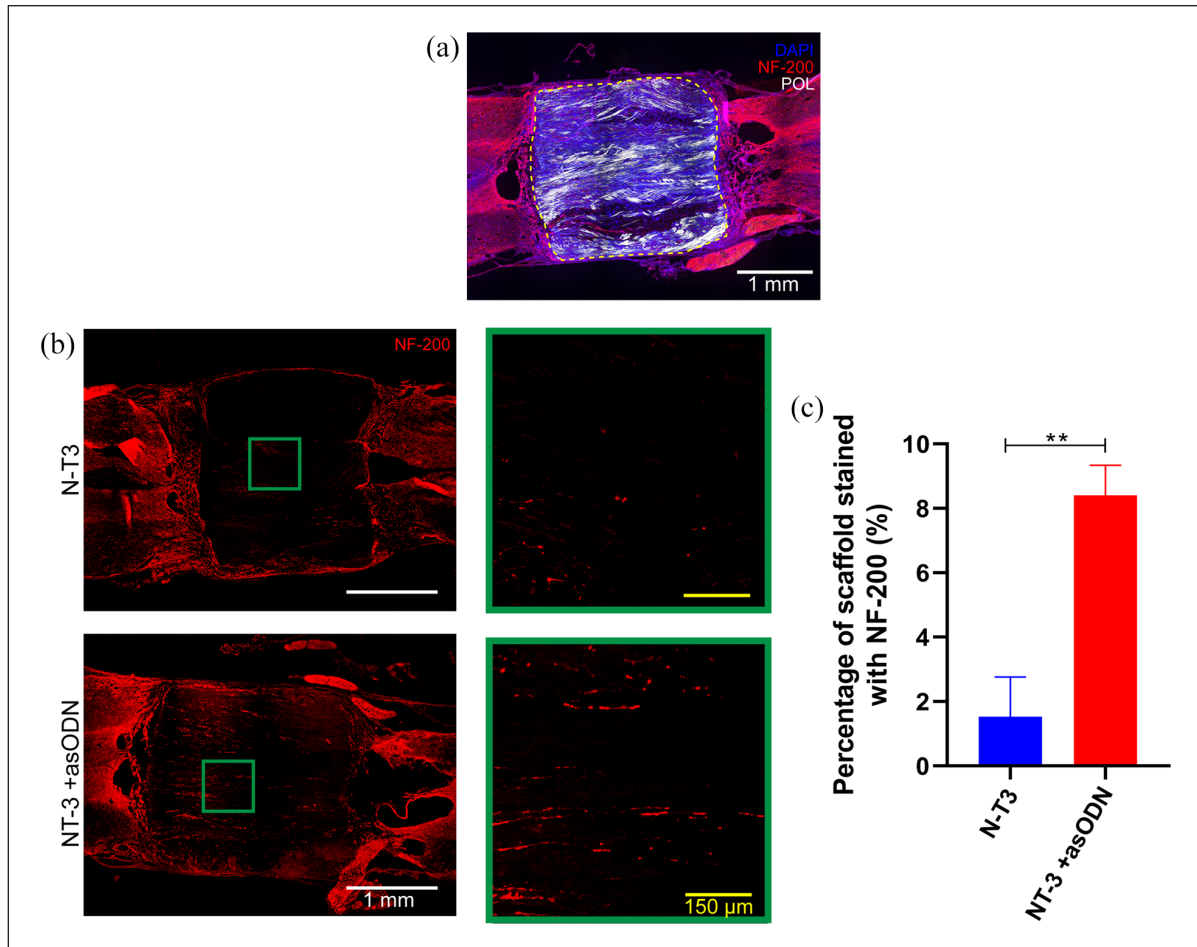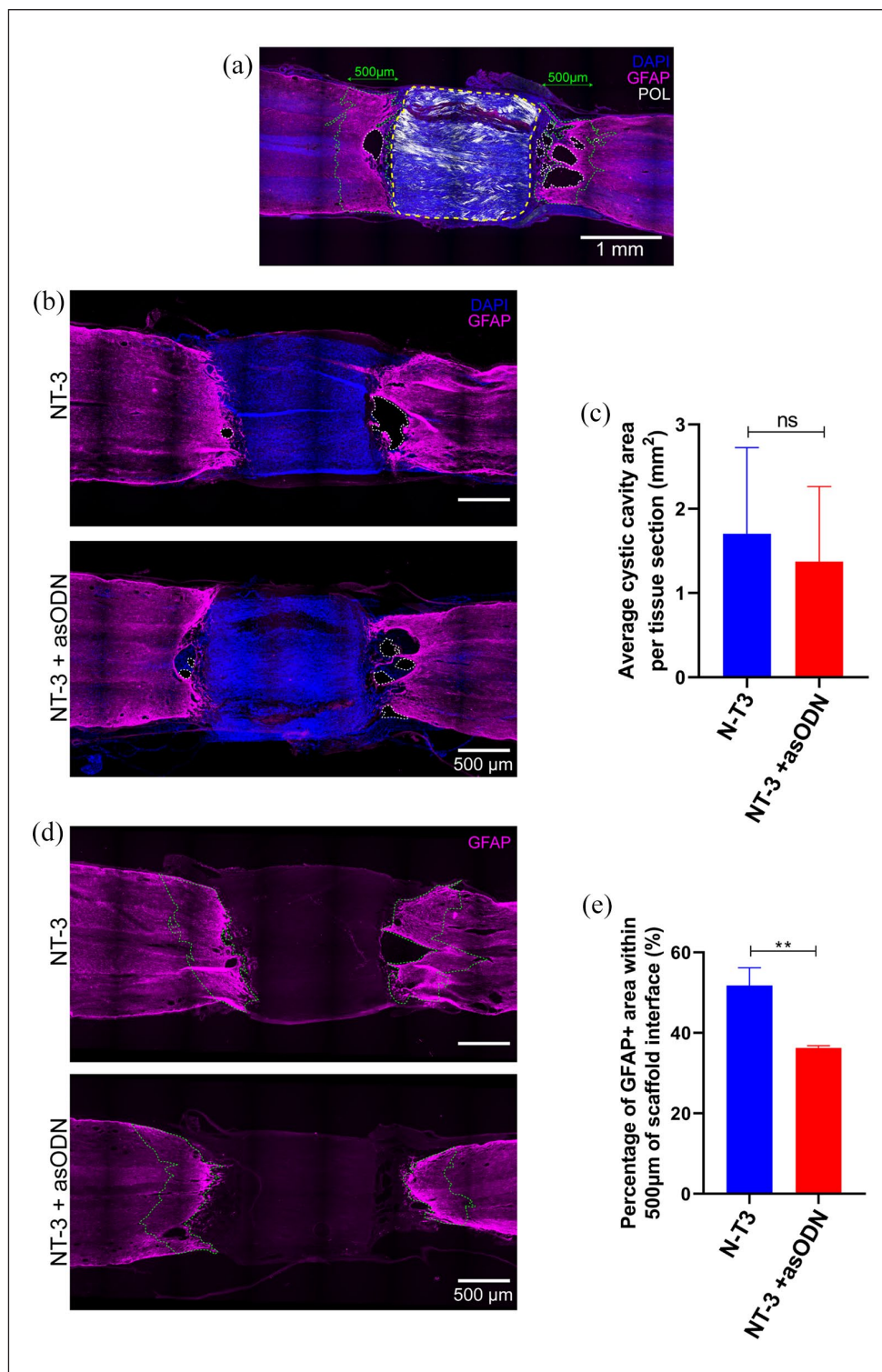
Figure 3. asODN stimulated axonal ingrowth into scaffolds 4 weeks after SCI. (a) Representative fluorescent microscopy image of fibre-hydrogel scaffold implanted at injury site. Yellow dotted line demarcates boundary of scaffold. (b) Representative fluorescent microscopy images of NF-200 (red) expression at injury site. Green boxes represent the magnified regions. (c) Quantification of the percentage of scaffold stained with NF-200. Data suggested that the presence of asODN promoted axonal ingrowth after SCI. Mann Whitney test ($n = 3$, where n represents 1 biological repeat). **: $p < 0.01$.

Moreover, SCI repair involves tissue reconstruction, which requires a scaffold instead of carriers to facilitate the process. Consequently, our success in adopting Cx43asODN-coated electrospun collagen scaffolds for skin wound healing[49] has inspired the use of electrospun scaffolds for the delivery of asODNs to SCI sites. Electrospinning is a versatile fabrication technique that could allow scaffolds of various morphologies to be manufactured.[50] Hence, we believe that electrospun scaffolds could potentially be designed and fabricated for delivery of asODNs to SCI sites.

In this respect, the scaffold used in this study contained two crucial features, aligned electrospun fibres and collagen hydrogel. This design was adopted from our previous studies where aligned electrospun fibres were crucial in providing topographical guidance for axonal extension.[32–34] To mimic the natural extracellular matrix while allowing cell infiltration and sufficient nutrient exchange, these fibres were physically supported in 3D conformation by the surrounding

lyophilised collagen hydrogel – a highly porous matrix. Beyond providing fibres with physical support, the collagen hydrogel was crucial for the localised sustained delivery of Cx43asODNs (Figure 1(f)). After a complete transection of adult spinal cord, Cx43 expression levels were reported to be upregulated within hours and reaching over three times normal levels at 4 weeks post-injury.[51] Localised sustained delivery of asODNs, in the presence of NT-3, via fibre-hydrogel scaffold successfully reduced Cx43 expression *in vivo* for at least 4 weeks despite the release kinetics of asODNs *in vitro* – burst release of asODNs for the first 3 days and this release plateaued at Day 25 (Figures 1(f) and 5(c)). Such sustained delivery of asODN could be crucial for long-term downregulation or preventing upregulation of Cx43 at the injury site to reduce secondary damage after SCI. On the other hand, although the release kinetics of NT-3 was not examined in this work, we would expect a similar release behavior as our previous study where sustained

Figure 4. Effect of asODN on cyst formation and glial scar modulation 4 weeks after SCI. (a) Representative fluorescent microscopy image of fibre-hydrogel scaffold implanted at injury site. Yellow dotted line demarcates boundary of scaffold. White dotted line traces the boundary of a cyst. Green dotted line marks the area where GFAP was quantified. (b) Representative fluorescent microscopy images of DAPI (blue) and GFAP (magenta) expression at injury site. The area that is void of cells (i.e. no DAPI expression) was defined as a cyst. (c) Quantification of average cystic cavity area per tissue section. No significant reduction in cystic cavity area was observed with asODN treatment. Mann Whitney test ($n = 3$, where n represents 1 biological repeat). ns: not significant, $p = 0.8701$. (d) Representative fluorescent microscopy images of GFAP (magenta) expression at injury site. (e) Quantification of the percentage area of GFAP+ within 500 μm of scaffold interface. Data suggested that the presence of asODN reduced astrocyte activation after SCI. Mann Whitney test ($n = 3$, where n represents 1 biological repeat). **: $p < 0.01$.
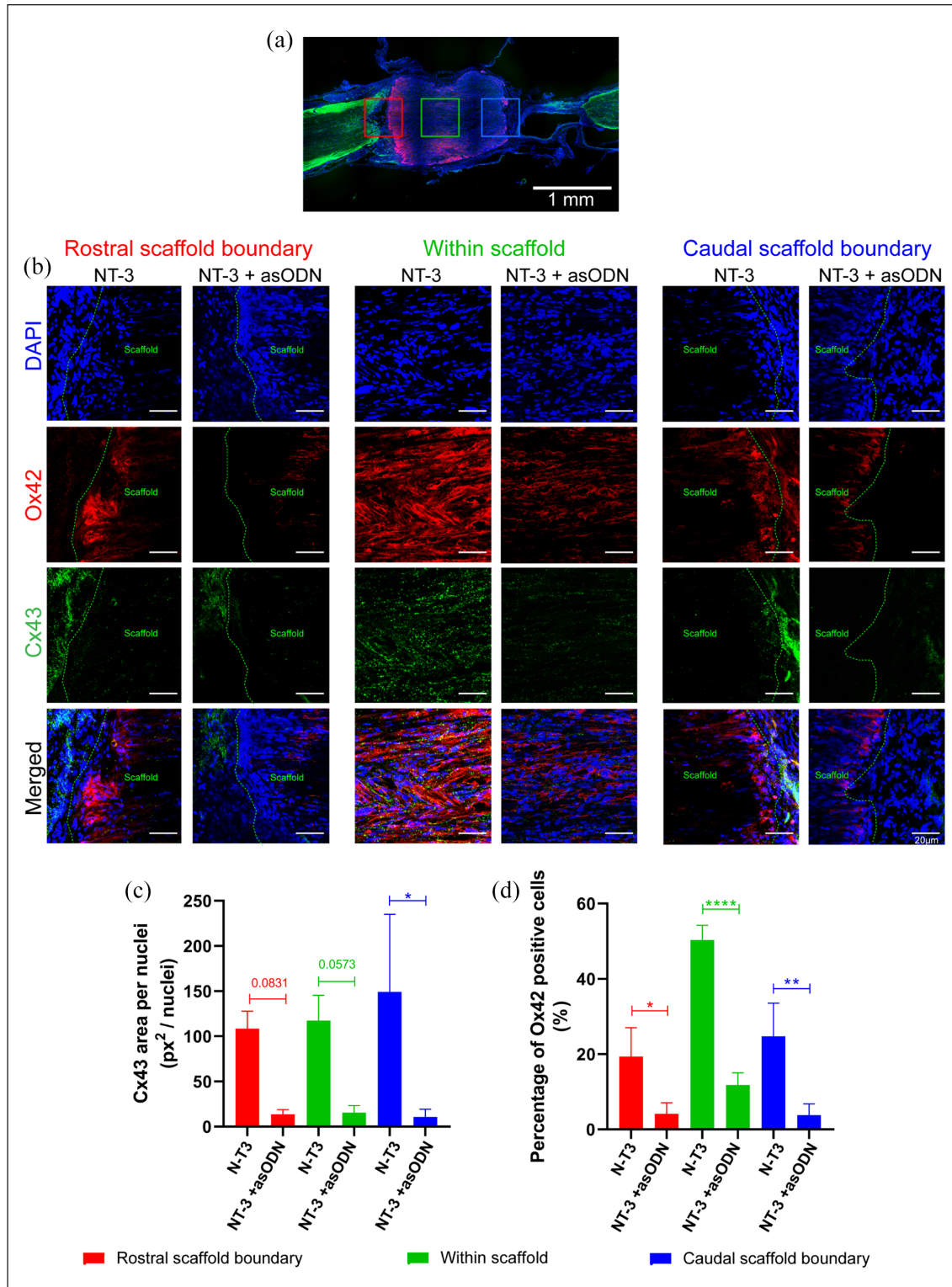
Figure 5. Reduction of Cx43 expression with asODN treatment decreased microglial activation after SCI. (a) Fluorescent microscopy image of a spinal cord section, with scaffold implanted at injury site, as a representative image to show regions imaged by confocal microscopy. Red box: Rostral scaffold boundary. Green box: Within scaffold. Blue box: Caudal scaffold boundary. (b) Representative confocal microscopy images of Ox42 (red) and Cx43 (green) expression at the three defined regions of interests. Green dotted line marks the scaffold boundary. (c) Quantification of Cx43 area per nuclei. Data suggested that expression of Cx43 was significantly reduced with asODN treatment 4 weeks after SCI. Mann Whitney test ($n = 3$, where n represents 1 biological repeat). *: $p < 0.05$. (d) Quantification of Ox42 positive cells. Data suggested a significant decrease in microglial cells at injury site with asODN treatment. Mann Whitney test ($n = 3$, where n represents 1 biological repeat). *: $p < 0.05$. **: $p < 0.01$. ****: $p < 0.0001$.

release of NT-3 over 90 days with a burst release within the first 3 days was observed.[32] Of note, such in vitro release kinetics of asODNs might not precisely mimic the release of asODNs at the injury site. The constant replacement of PBS during the in vitro release kinetics promotes a greater extent of asODN release from the scaffold. While there are differences to be expected in the release kinetics of asODNs at the injury site, the in vitro release kinetics study conducted could still provide insights to the release of asODNs from our fibre-hydrogel scaffold.

Notably, Cx43asODNs were delivered from the fibre-hydrogel scaffolds in the absence of any transfection reagent. This approach follows the success achieved in our previous work. Specifically, naked Cx43asODNs, delivered via F127 Pluronic gel, penetrated into the dorsal grey matter of an uninjured rat spinal cord and transiently downregulated the expression of Cx43 for up to 8h.[52] Similarly, Cx43 expression was also successfully downregulated when naked Cx43asODNs were delivered into the skin wound bed either with F127 Pluronic gel[31] or electrospun collagen scaffolds.[59] The absence of transfection reagents could potentially minimise the difficulties during subsequent translation into humans.

Interestingly, although the fibre bundle was embedded within a porous collagen hydrogel matrix, we did not observe any negative impact of the surrounding structure on the fibres (Figure 1(d)). Since this matrix surrounds the fibre bundle, the collagen hydrogel does not block the growth of the axon descending from the grey matter. On the other hand, we are unable to conclude if the collagen matrix gets resorbed during the tissue repair process. However, from the H&E images in Figure 2(a), a proteinaceous matrix (stained with eosin) can still be observed around the fibre bundle. Therefore, complete resorption of the collagen matrix 4 weeks after scaffold implantation seems unlikely.

In this work, the polymer used was poly (caprolactone-co-ethyl ethylene phosphate) (PCLEEP) copolymer. PCLEEP has higher degradation rate in comparison to poly (caprolactone) (PCL).[53] Since the fibre-hydrogel scaffold is a temporary matrix to encourage axon regeneration and the eventual reconnection of the neuronal circuit, a polymer with faster degradation rate would be more ideal for the tissue repair application here.

In spinal cord transection injury models, neuronal loss was initially confined to the primary lesion site.[54] However, 6 h post-injury, severely damaged neurons appeared within an area about 800 μm away.[54] This area of cell loss increased as time progressed.[54,55] Hence, to understand the neuroprotective effects of Cx43asODN at 4 weeks post-injury, we examined H&E-stained spinal cord sections at two regions, 200 μm away and 1 mm away from the scaffold border (Figure 2(a)). The former being near to the primary lesion site while the latter would shed more light into any possible secondary damage to neurons further away from this primary lesion site. In addition, 200 μm away from the

scaffold was selected as our previous study, using the same scaffold design,[32] found that nucleic acids were taken up by cells in the surrounding tissues, up to a distance of 300 μm. When comparing these regions, we observed significant difference in neuronal cell morphology between the treatments. In the presence of Cx43asODNs, the shape of neurons remained distinct even in further away regions from the primary lesion site, that is, 1 mm away. This observation is true at both caudal and rostral ends (Figure 2(b)). However, in the absence of Cx43asODNs, neurons were observed to have lost their distinct morphology and their cytoplasm appeared to be less intense for the eosin stain (Figure 2(b)). Furthermore, the number of neurons were reduced in the absence of Cx43asODNs especially near the primary lesion site, that is, 200 μm away from the scaffold (Figure 2(b) and (c)). Both the loss of neurons and changes in neuron morphology are consistent with literature that report the fate of neurons after traumatic spinal cord injury in rats.[54] We speculate that the preservation of neurons, in the Cx43asODN treated tissues, could be due to the downregulation of Cx43 protein expression or preventing its upregulation. The absence or blockage of Cx43 hemichannels after SCI reduced the presence of small molecules, such as glutamate, potassium ions, nitric oxide, and reactive oxidative species (ROS), in the extracellular space – all of which in excessive amounts are found to be toxic to neurons.[56,57]

Neuron preservation is crucial after SCI as the surviving neurons can support axon regeneration into the injury site.[58] Indeed, when examining the axonal ingrowth within the NT-3 + Cx43asODN scaffolds, more NF-200 signals were observed (Figure 3(b) and (c)). Axonal ingrowth within the scaffold was also observed to be guided along the aligned fibres, an observation that is consistent with our previous work where the same scaffold design was adopted.[32–34] Although NT-3 has been reported to encourage neuronal survival and axon regeneration, we did not observe significant neuron preservation or axonal ingrowth in the scaffold. This limited axonal ingrowth is consistent with our previous work where NT-3 alone was insufficient to promote significant axonal extension and other molecular interventions were required to stimulate extension of axons.[34] We speculate that the lack of robust axonal ingrowth into our electrospun fiber hydrogel scaffolds, even in the presence of NT-3, could be due to insufficient biochemical signaling.[62,63] This, however, could be resolved either through the synergistic use of appropriate microRNAs 34 or as shown in this study, the inclusion of antisense Cx43.

Interestingly, although the Cx43asODN treatment preserved neurons even up to 1 mm away from the scaffold boundary, we did not observe any differences in NF-200 signals along the intact spinal cord tissue. This observation is contrary to existing literature where axonal degeneration and neuronal death are closely related.[58] We speculate that the extent of axonal degeneration might not be obvious at

4 weeks post-injury. Longer time points might be needed to observe such differences.

In addition to enhancing axonal ingrowth, NT-3 + Cx43asODN scaffolds also tended to reduce glial scarring at the lesion site 4 weeks post-injury. Astrocytes are major component of the glial scar.[59] They are predominantly interconnected by Cx43 gap junction proteins.[8,10,60] Reactive astrocytes enveloping both brain and spinal cord lesions showed significant upregulation in their Cx43 expression.[6,9,61] Here, GFAP was used as a marker to study astrocytes. Of note, both resting and activated astrocytes express GFAP. However, increased GFAP expression is known and associated with astrocyte activation.[67] In our work, reduced presence of reactive astrocytes was observed in associated with reduced GFAP expression, up to 500 μm away from the scaffold boundary, with asODN treatment. We speculate that the downregulation or preventing upregulation of Cx43 protein expression, as a result of the Cx43asODN treatment, could have reduced the proliferation of reactive astrocytes and prevented the formation of larger glial scars.[64–66] On the other hand, no significant difference in cystic cavity formation between the treatments were observed. This could be attributed to the severity of the injury model that disrupted the overlaying vasculature crucial to reduce cyst formation after complete spinal cord transection in rats.[68]

Phagocytes accumulating at CNS injury sites are typically from two sources – resident microglia that proliferate at the site and circulatory macrophages that are recruited from the bloodstream.[69] Upon spinal cord injury, resting microglial become activated in response to the pro-inflammatory cytokines.[70] Activated microglia further release a wide range of pro-inflammatory signals and substances that are toxic to neurons including ROS, proteases, and cytokines.[43,44] Upon activation, microglia were found to express Cx43.[11] In particular, activated microglia were observed to be coupled to each other via Cx43 gap junctions and thereby, facilitating the spread of activation further from the lesion site.[71,72] In this work, we observed reduced Cx43 protein expression even at 4 weeks post scaffold implantation. The localised sustained delivery of Cx43asODN provided by the scaffolds could have facilitated this extended period of downregulation or prevented upregulation of Cx43 protein expression. This reduction in Cx43 protein expression was concurrently observed with reduced microglial activation. In particular, in the presence of Cx43asODNs, microglia within the scaffold appeared stellate, a stark contrast to the activated microglia in the NT-3 treatment group that appeared rounded. Besides downregulating Cx43 expression of activated microglia residing at the injury site, the sustained delivery of Cx43asODNs to the injury site could have also downregulated Cx43 expression in recruited microglia. This could have further suppressed the activation of microglia as observed from our work.

After SCI, Cx43 expression increases within 4 h and triples the normal levels at 4 weeks post injury – Cx43 mRNA expression was observed to be in an upward trend even on the fourth week possibly suggesting continuous upregulated Cx43 expression[53]. Previously, asODN treatment was shown to downregulate connexin expression transiently thereby reducing connexin signalling detrimental during the early injury phase[55]. Consequently, connexin expression and gap junction communication were both recovered after this transient downregulation to facilitate the recovery of the tissue[55]. Here, given the burst release of asODNs in the first 3 days, the neuroprotection and reduction of secondary damages could have been primarily conferred and mitigated during these 3 days. Cx43 expression would have increased after the first 3 days possibly either due to the ongoing inflammatory response to clear out cellular debris or to facilitate the recovery process[55,76]. Nonetheless, the scaffold delivery system in this work continuously delivered low levels of asODN to the injury site in hopes of keeping Cx43 expression low but not completely absent.

Although several studies have already shown the positive wound healing effects of downregulating Cx43 on SCI, these have heavily relied on F127 Pluronic gel as the delivery vehicle.[11,73] When placed on an injured spinal cord, F127 Pluronic gel degraded within 24 h.[11] Hence, the downregulation of Cx43 was limited to the _in vivo_ half-life of F127 Pluronic gel.[11] In this work, the fibre-hydrogel scaffold provided topographical cues to guide axon ingrowth while downregulating Cx43 protein expression over extended periods of time to mitigate the spread of pro-inflammatory mediators and cell death signals. Here, the collagen hydrogel serves primarily as the delivery vehicle of the Cx43-specific asODNs. Although sustained released was observed, the rapid release of the asODNs could be attributed to the physically crosslinked collagen matrix which loosely encapsulated these asODNs. To slow down the release of asODNs, the collagen matrix could be chemically crosslinked through the incorporation of glutaraldehyde or polyethylene glycol.[74] However, a stiffer matrix might induce severe glial scarring[75] which could counteract the benefits of the asODNs.

Of note, the reduction in secondary damages with Cx43asODNs were all observed in the presence of NT-3. In our previous work[33], NT-3 is needed for signs of NF ingrowth into the scaffold at the injury site. Poor NF regeneration was observed in the absence of NT-3. Thereafter, in all our works, NT-3 has been our baseline. However, the inclusion of NT-3 in the scaffold could have already substantially reduced GFAP-positive reactive astrocytes and activated microglial even in the absence of Cx43asODNs[78]. Future work can perhaps look into setting up additional treatment groups to compare how Cx43asODNs and NT-3 can individually mitigate such secondary damages. Additional work can also explore if there are any synergistic effects when both Cx43asODNs and NT-3 are being treated on an SCI site.

Within the scope of this work, a relatively shorter time point (4 weeks post injury) was chosen here to give early

indications of the use of scaffolds to deliver Cx43-specific antisense oligodeoxynucleotides for the modulation of secondary neuronal damage while promoting and guiding axonal outgrowth from the injury border. Given such early time points, conducting functional studies would not be helpful given the severity of the injury model (i.e. complete transection). Hence, we decided to explore functional studies in our future work instead where longer time points will be considered. When compared to previous work where functional studies was conducted at 4 weeks post injury[79], the extent of NF ingrowth in the scaffold in this study, in the presence of both NT-3 and Cx43 asODNs, likely would not be sufficient to yield any difference in functional outcome when compared to the NT-3 treated group. Nonetheless, here in our work, Cx43 asODNs reduced neuronal death and glial scarring. Thus, we speculate that Cx43 asODNs could be adopted synergistically with NT-3 to enhance regeneration while resulting in functional outcome should longer timepoints be included in future studies.

While positive outcomes were observed with these Cx43asODNs loaded fibre-hydrogel scaffold, these scaffolds were implanted at the injury site immediately – unlike in humans.[77] Clinically, SCI patients often do not receive immediate medical interventions. Hence, the results from this study will either need further validation from larger species (e.g. in mammals) or the experimental setup, in terms of the surgical workflow, will need alterations to improve clinical relevance upon translation to patients. Of note, the use of this scaffold construct might not be limited for application within the acute phase. Treatment of injury at the chronic phase could be possible with the removal of glial scar tissue which would elicit fresh lesion response (i.e. acute phase) while creating a physical space for the scaffold to be implanted. Moreover, sustained overexpression of Cx43 would be expected at the chronic phase of SCI 53 and hence, the initial burst release of asODNs, upon the scaffold implantation, could be crucial to prevent further neuronal loss and alleviate the ongoing inflammatory responses.

Concurrently, more in-depth studies on other cell types (e.g. endothelial cells) could be explored in the future to understand how sustained downregulation of Cx43 protein can encourage healing after SCI. This work can also be expanded, in the future, to include both early (e.g. 2 weeks) and late (e.g. 3 months) time points to study the changes Cx43 expression at the injury site and the functional recovery outcome. In addition, future work can place more emphasis on showing quantitative results based on molecular biology to strengthen our current findings. To improve the existing platform, active delivery mechanisms (e.g. stimuli-triggered release of Cx43asODNs) could also be incorporated to better cater to the needs of the injury site.

Conclusion

Our study reflects the potency of sustained Cx43asODN delivery, in the presence of NT-3, via scaffolds in offering neuroprotection after spinal cord injury. In addition, the use of the fibre-hydrogel scaffold has offered contact guidance to axons, guiding axonal regeneration into the lesion site. This work has also further established the positive effects of downregulating Cx43 protein expression after SCI injury, reduction in glial scarring and modulating microglial activation.

Author's note

David L Becker is also affiliated to National Skin Center, 1 Mandalay Road, Singapore.

Author contributions

JS Chin and U. Milbreta carried out the experiments. JS Chin wrote the manuscript with support from D. Becker and SY Chew. JS Chin fabricated the scaffolds. JS Chin analysed all experimental data with support from U. Milbreta, D. Becker and SY Chew. D. Becker and SY Chew supervised the project.

ORCID iD

Sing Yian Chew (iD) https://orcid.org/0000-0002-6084-5967

References

1. Kielian T. Glial connexins and gap junctions in CNS inflammation and disease. *J Neurochem* 2008; 106: 1000–1016.
2. Willecke K, Eiberger J, Degen J, et al. Structural and functional diversity of connexin genes in the mouse and human genome. *Biol Chem* 2002; 383: 725–737.
3. Ratkay-Traub I, Hopp B, Bor Z, et al. Regeneration of rabbit cornea following excimer laser photorefractive keratectomy: a study on gap junctions, epithelial junctions and epidermal growth factor receptor expression in correlation with cell proliferation. *Exp Eye Res* 73: 291–302.
4. Wang CM, Lincoln J, Cook JE, et al. Abnormal connexin expression underlies delayed wound healing in diabetic skin. *Diabetes*. Epub ahead of print 2007. DOI: 10.2337/db07-0613
5. Ohsumi A, Nawashiro H, Otani N, et al. Alteration of gap junction proteins (connexins) following lateral fluid percussion injury in rats. *Acta Neurochir Suppl* 2006; 96: 148–150.

6. Huang C, Han X, Li X, et al. Critical Role of Connexin 43 in secondary expansion of traumatic spinal cord injury. *J Neurosci* 2012; 32: 3333–3338.

7. Umebayashi D, Natsume A, Takeuchi H, et al. Blockade of gap Junction hemichannel protects secondary spinal cord injury from activated microglia-mediated glutamate exitoneurotoxicity. *J Neurotrauma* 2014; 31: 1967–1974.

8. Freitas-Andrade M and Naus CC. Astrocytes in neuroprotection and neurodegeneration: the role of connexin43 and pannexin1. *Neuroscience* 2016; 323: 207–221.

9. O'Carroll SJ, Gorrie CA, Velamoor S, et al. Connexin43 mimetic peptide is neuroprotective and improves function following spinal cord injury. *Neurosci Res* 2013; 75: 256–267.

10. Nagy JI and Rash JE. Connexins and gap junctions of astrocytes and oligodendrocytes in the CNS. *Brain Res Rev* 2000; 32: 29–44.

11. Cronin M, Anderson PN, Cook JE, et al. Blocking connexin43 expression reduces inflammation and improves functional recovery after spinal cord injury. *Mol Cell Neurosci* 2008; 39: 152–160.

12. Giaume C and Liu X. From a glial syncytium to a more restricted and specific glial networking. *J Physiol Paris* 2012; 106: 34–39.

13. Brambilla R, Bracchi-Ricard V, Hu WH, et al. Inhibition of astroglial nuclear factor kappaB reduces inflammation and improves functional recovery after spinal cord injury. *J Exp Med* 2005; 202: 145–156.

14. Fitch MT, Doller C, Combs CK, et al. Cellular and molecular mechanisms of glial scarring and progressive cavitation: in vivo and in vitro analysis of inflammation-induced secondary injury after CNS trauma. *J Neurosci* 1999; 19: 8182–8198.

15. Chen MJ, Kress B, Han X, et al. Astrocytic CX43 hemichannels and gap junctions play a crucial role in development of chronic neuropathic pain following spinal cord injury. *Glia* 2012; 60: 1660–1670.

16. Sun L, Gao J, Zhao M, et al. A novel cognitive impairment mechanism that astrocytic p-connexin 43 promotes neuronic autophagy via activation of P2X7R and down-regulation of GLT-1 expression in the hippocampus following traumatic brain injury in rats. *Behav Brain Res* 291: 315–324.

17. Castellano P and Eugenin EA. Regulation of gap junction channels by infectious agents and inflammation in the CNS. *Front Cell Neurosci* 2014; 8: 122.

18. Chew SS, Johnson CS, Green CR, et al. Role of connexin43 in central nervous system injury. *Exp Neurol* 2010; 225: 250–261.

19. Evans WH, De Vuyst E and Leybaert L. The gap junction cellular internet: Connexin hemichannels enter the signalling limelight. *Biochem J* 2006; 397: 1–14.

20. Puil E and El-Beheiry H. Anaesthetic suppression of transmitter actions in neocortex. *Br J Pharmacol* 1990; 101: 61–66.

21. Kress HG and Tas PW. Effects of volatile anaesthetics on second messenger ca in neurones and non-muscular cells. *Br J Anaesth* 1993; 71: 47–58.

22. Law LY, Zhang WV, Stott NS, et al. In vitro optimization of antisense oligodeoxynucleotide design: an example using the connexin gene family. *J Biomol Tech* 2006; 17: 270–282.

23. Phillips MI and Zhang YC. Basic principles of using antisense oligonucleotides in vivo. *Meth Enzymol* 2000; 313: 46–56.

24. Theriault E, Frankenstein UN, Hertzberg EL, et al. Connexin43 and astrocytic gap junctions in the rat spinal cord after acute compression injury. *J Comp Neurol* 1997; 382: 199–214.

25. Oguro K, Jover T, Tanaka H, et al. Global ischemia-induced increases in the gap junctional proteins connexin 32 (Cx32) and Cx36 in hippocampus and enhanced vulnerability of Cx32 knock-out mice. *J Neurosci* 2001; 21: 7534–7542.

26. Falzarano MS, Passarelli C and Ferlini A. Nanoparticle delivery of antisense oligonucleotides and their application in the exon skipping strategy for duchenne muscular dystrophy. *Nucleic Acid Ther* 2014; 24: 87–100.

27. Stein CA. Eteplirsen approved for duchenne muscular dystrophy: the FDA faces a difficult choice. *Mol Ther* 2016; 24: 1884–1885.

28. Adams D, Gonzalez-Duarte A, O'Riordan WD, et al. Patisiran, an RNAi therapeutic, for hereditary transthyretin amyloidosis. *N Engl J Med* 2018; 379: 11–21.

29. Yang L, Ma F, Liu F, et al. Efficient delivery of antisense oligonucleotides using bioreducible lipid nanoparticles in vitro and in vivo. *Mol Ther Nucleic Acids* 2020; 19: 1357–1367.

30. Juliano RL. The delivery of therapeutic oligonucleotides. *Nucleic Acids Res* 2016; 44: 6518–6548.

31. Qiu C, Coutinho P, Frank S, et al. Targeting Connexin43 Expression Accelerates the Rate of Wound Repair. *Curr Biol*. Epub ahead of print 2003. DOI: 10.1016/j.cub.2003.09.007.

32. Nguyen LH, Gao M, Lin J, et al. Three-dimensional aligned nanofibers-hydrogel scaffold for controlled non-viral drug/gene delivery to direct axon regeneration in spinal cord injury treatment. *Sci Rep* 2017; 7: 42212.

33. Milbreta U, Nguyen LH, Diao H, et al. Three-dimensional nanofiber hybrid scaffold directs and enhances axonal regeneration after spinal cord injury. *ACS Biomater Sci Eng* 2016; 2: 1319–1329.

34. Zhang N, Milbreta U, Chin JS, et al. Biomimicking Fiber Scaffold as an Effective In Vitro and In Vivo MicroRNA Screening Platform for Directing Tissue Regeneration. *Adv Sci*. Epub ahead of print 2019. DOI: 10.1002/advs.201800808.

35. Wang YC, Li Y, Yang XZ, et al. Tunable thermosensitivity of biodegradable polymer micelles of poly(ε-caprolactone) and polyphosphoester block copolymers. *Macromolecules* 2009; 42: 3026–3032.

36. Di Fiore MSH. Atlas of Human Histology. *Am J Med Sci* 1967; 254: 915.

37. Hakim JS, Esmaeili Rad M, Grahn PJ, et al. Positively Charged Oligo[Poly(Ethylene Glycol) Fumarate] Scaffold Implantation Results in a Permissive Lesion Environment after Spinal Cord Injury in Rat. Tissue Eng - Part A. Epub ahead of print 2015. DOI: 10.1089/ten.tea.2015.0019.

38. Garman RH. Histology of the Central Nervous System. *Toxicologic Pathology*. Epub ahead of print 2011. DOI: 10.1177/0192623310389621.

39. Hollis ER and Tuszynski MH. Neurotrophins: potential therapeutic tools for the treatment of spinal cord injury. *Neurother* 2011; 8: 694–703.

40. Schnell L, Schneider R, Kolbeck R, et al. Neurotrophin-3 enhances sprouting of corticospinal tract during development and after adult spinal cord lesion. *Nature* 1994; 367: 170–173.

41. Jurga AM, Paleczna M, Kuter KZ. Overview of General and Discriminating Markers of Differential Microglia Phenotypes. Front Cell Neurosci. Epub ahead of print 2020. DOI: 10.3389/fncel.2020.00198.

42. Liu Y, Kelamangalath L, Kim H, et al. NT-3 promotes proprioceptive axon regeneration when combined with activation of the mTor intrinsic growth pathway but not with reduction of myelin extrinsic inhibitors. *Exp Neurol* 2016 283: 73–84.

43. Gajardo-Gómez R, Labra VC and Orellana JA. Connexins and pannexins: New insights into microglial functions and dysfunctions. *Front Mol Neurosci* 2016; 9: 86.

44. Pearse DD, Pereira FC, Stolyarova A, et al. Inhibition of tumour necrosis factor-alpha by antisense targeting produces immunophenotypical and morphological changes in injury-activated microglia and macrophages. *Eur J Neurosci* 2004; 20: 3387–3396.

45. Profyris C, Cheema SS, Zang D, et al. Degenerative and regenerative mechanisms governing spinal cord injury. *Neurobiol Dis* 2004; 15: 415–436.

46. Lin JH, Weigel H, Cotrina ML, et al. Gap-junction-mediated propagation and amplification of cell injury. *Nat Neurosci* 1998; 1: 494–500.

47. Fehlings MG and Baptiste DC. Current status of clinical trials for acute spinal cord injury. *Injury* 2005; 36 Suppl 2: B113–B122.

48. Nesathurai S. Steroids and spinal cord injury: revisiting the NASCIS 2 and NASCIS 3 trials. *J Trauma Inj Infect Crit Care* 1998; 45: 1088–1093.

49. Gilmartin DJ, Soon A, Thrasivoulou C, et al. Sustained release of Cx43 antisense oligodeoxynucleotides from coated collagen scaffolds promotes wound healing. *Adv Healthc Mater* 2016; 5: 1786–1799.

50. Pham QP, Sharma U and Mikos AG. Electrospinning of polymeric nanofibers for tissue engineering applications: a review. *Tissue Eng* 2006; 12: 1197–1211.

51. Lee IH, Lindqvist E, Kiehn O, et al. Glial and neuronal connexin expression patterns in the rat spinal cord during development and following injury. J Comp Neurol. Epub ahead of print 2005. DOI: 10.1002/cne.20567.

52. Cronin M, Anderson PN, Green CR, et al. Antisense delivery and protein knockdown within the intact central nervous system. *Front Biosci* 2006; 11: 2967–2975.

53. Chew SY, Wen J, Yim EK, et al. Sustained release of proteins from electrospun biodegradable fibers. *Biomacromolecules* 2005; 6: 2017–2024.

54. Dusart I and Schwab ME. Secondary cell death and the inflammatory reaction after dorsal hemisection of the rat spinal cord. *Eur J Neurosci* 1994; 6: 712–724.

55. Siebert JR, Middelton FA and Stelzner DJ. Intrinsic response of thoracic propriospinal neurons to axotomy. *BMC Neurosci* 2010; 11: 69.

56. Orellana JA, Sáez PJ, Shoji KF, et al. Modulation of brain hemichannels and gap junction channels by pro-inflammatory agents and their possible role in neurodegeneration. *Antioxid Redox Signal* 2009; 11: 369–399.

57. Almad AA, Doreswamy A, Gross SK, et al. Connexin 43 in astrocytes contributes to motor neuron toxicity in myotrophic lateral sclerosis. *Glia* 2016; 64: 1154–1169.

58. Rodemer W and Selzer ME. Role of axon resealing in retrograde neuronal death and regeneration after spinal cord injury. *Neural Regen Res* 2019; 14: 399–404.

59. Stichel CC, Lausberg F, Hermanns S, et al. Scar modulation in subacute and chronic CNS lesions: Effects on axonal regeneration. *Restor Neurol Neurosci* 1999; 15: 1–15.

60. Nagy JI, Dudek FE and Rash JE. Update on connexins and gap junctions in neurons and glia in the mammalian nervous system. *Brain Res Rev* 2004; 47: 191–215.

61. Nakase T, Yoshida Y and Nagata K. Enhanced connexin 43 immunoreactivity in penumbral areas in the human brain following ischemia. *Glia* 2006; 54: 369–375.

62. Li G, Che MT, Zhang K, et al. Graft of the NT-3 persistent delivery gelatin sponge scaffold promotes axon regeneration, attenuates inflammation, and induces cell migration in rat and canine with spinal cord injury. *Biomaterials*. Epub ahead of print 2016. DOI: 10.1016/j.biomaterials.2015.11.059.

63. Yang Z, Zhang A, Duan H, et al. NT3-chitosan elicits robust endogenous neurogenesis to enable functional recovery after spinal cord injury. *Proc Natl Acad Sci U S A*. Epub ahead of print 2015. DOI: 10.1073/pnas.1510194112.

64. Lee CY, Pappas GD, Kriho V, et al. Proliferation of a subpopulation of reactive astrocytes following needle-insertion lesion in rat. *Neurol Res* 2003; 25: 767–776.

65. Scemes E, Duval N and Meda P. Reduced expression of P2Y1 receptors in connexin43-null mice alters calcium signaling and migration of neural progenitor cells. *J Neurosci* 2003; 23: 11444–11452.

66. Haupt C, Witte OW and Frahm C. Up-regulation of Connexin43 in the glial scar following photothrombotic ischemic injury. *Mol Cell Neurosci* 2007; 35: 89–99.

67. Liddelow SA, Barres BA. Reactive Astrocytes: Production, Function, and Therapeutic Potential. *Immunity* 2017; 46: 957–967.

68. Rooney GE, Endo T, Ameenuddin S, et al. Importance of the vasculature in cyst formation after spinal cord injury: Laboratory investigation. *J Neurosurg Spine* 2009; 11: 432–437.

69. Katsumoto A, Lu H, Miranda AS, et al. Ontogeny and functions of central nervous system macrophages. *J Immunol* 2014; 193: 2615–2621.

70. Hinkerohe D, Smikalla D, Haghikia A, et al. Effects of cytokines on microglial phenotypes and astroglial coupling in an inflammatory coculture model. *Glia* 2005; 52: 85–97.

71. Eugenín EA, Brañes MC, Berman JW, et al. TNF-alpha plus IFN-gamma induce connexin43 expression and formation of gap junctions between human monocytes/macrophages that enhance physiological responses. *J Immunol* 2003; 170: 1320–1328.

72. Amat JA, Ishiguro H, Nakamura K, et al. Phenotypic diversity and kinetics of proliferating microglia and astrocytes following cortical stab wounds. *Glia* 1996; 16: 368–382.

73. O'Carroll SJ, Alkadhi M, Nicholson LF, et al. Connexin 43 mimetic peptides reduce swelling, astrogliosis, and neuronal cell death after spinal cord injury. *Cell Commun Adhes* 2008; 15: 27–42.

74. Sarrigiannidis SO, Rey JM, Dobre O, et al. A tough act to follow: collagen hydrogel modifications to improve mechanical and growth factor loading capabilities. *Materials Today Bio* 2021; 10: 100098.

75. Hu Y, Huang G, Tian J, et al. Matrix stiffness changes affect astrocyte phenotype in an in vitro injury model. *NPG Asia Mater* 2021; 13: 35.

76. Xu CY, Zhang WS, Zhang H, et al. The Role of Connexin-43 in the Inflammatory Process: A New Potential Therapy to Influence Keratitis. *Journal of Ophthalmology*. Epub ahead of print 2019. DOI: 10.1155/2019/9312827.

77. Theodore N, Hlubek R, Danielson J, et al. First human implantation of a bioresorbable polymer scaffold for acute traumatic spinal cord injury: a clinical pilot study for safety and feasibility. *Neurosurg* 2016; 79: E305–E312.

78. Rao JS, Zhao C, Zhang A, et al. NT3-chitosan enables de novo regeneration and functional recovery in monkeys after spinal cord injury. *Proc Natl Acad Sci U S A*. Epub ahead of print 2018. DOI: 10.1073/pnas.1804735115.

79. Zhang N, Lin J, Lin VPH, et al. A 3D Fiber-Hydrogel Based Non-Viral Gene Delivery Platform Reveals that microRNAs Promote Axon Regeneration and Enhance Functional Recovery Following Spinal Cord Injury. *Adv Sci*. Epub ahead of print 2021. DOI: 10.1002/advs.202100805.